Available at
www.ElsevierMathematics.com
POWERED BY SCIENCE DIRECT®

Appl. Comput. Harmon. Anal. 15 (2003) 134–146

Applied and Computational Harmonic Analysis

www.elsevier.com/locate/acha

Letter to the Editor

On the chirp decomposition of Weierstrass–Mandelbrot functions, and their time–frequency interpretation

Pierre Borgnat and Patrick Flandrin *

Laboratoire de Physique (UMR 5672 CNRS), Ecole Normale Supérieure de Lyon, 46 allée d'Italie, 69364 Lyon cedex 07, France

Received 7 January 2003; accepted 15 February 2003

Communicated by Yves F. Meyer

Abstract

Weierstrass–Mandelbrot functions are given a time–frequency interpretation which puts emphasis on their possible decomposition on chirps as an alternative to their standard, Fourier-based, representation. Examples of deterministic functions are considered, as well as randomized versions for which the analysis is applied to empirical estimates of statistical quantities.

Keywords: Weierstrass function; Time–frequency; Mellin; Chirps

1. The Weierstrass–Mandelbrot function

In 1872, Weierstrass introduced a function defined by a semi-infinite superposition of weighted "tones" (or Fourier modes) whose frequencies are geometrically spaced, namely [22]:

$$W^*(t) = \sum_{n=0}^{\infty} \lambda^{-nH} \cos \lambda^n t, \tag{1}$$

with $\lambda > 1$ and $t \in \mathbb{R}$.

Assuming that the free parameter H, which governs the relative weights of the different tones, is such that $0 < H < 1$, the series given in (1) is convergent and the corresponding function $W^*(t)$, referred to as the *Weierstrass function* (WF), is a well-defined quantity. The point which has since then received

* Corresponding author.
E-mail addresses: pborgnat@ens-lyon.fr (P. Borgnat), flandrin@ens-lyon.fr (P. Flandrin).

1063-5203/$ – see front matter
doi:10.1016/S1063-5203(03)00047-2

much attention is that this function, although continuous, is nowhere differentiable: it is in fact Hölder continuous of order H everywhere [13]. As such, it has been widely used as a paradigmatic example of a fractal function, various measures of dimensions for its graph [3,8,16,21] ending up with the noninteger value $2-H$.

Despite its fractal structure, the WF is not truly H-self-similar since we only have $W^*(\lambda t) = \lambda^H[W^*(t) - \cos t] \neq \lambda^H W^*(t)$. This is so because the WF (1) is defined as a semi-infinite sum starting with $n = 0$, an operation which consists in adding frequencies $\omega \geqslant \lambda$ with no upper limit, but also with no spectral contributions below the lowest frequency defined by λ. The construction is therefore based on a *finite* larger scale which naturally prevents any form of *complete* scale invariance. This observation prompted Mandelbrot [16] (see also [17]) to modify the original definition (1) by adding in some suitable way the "missing" lower frequencies $\omega < \lambda$. His proposal was to generalize and complete (1) according to

$$W(t) = \sum_{n=-\infty}^{\infty} \lambda^{-nH}\left(1 - \mathrm{e}^{i\lambda^n t}\right)\mathrm{e}^{i\varphi_n}, \tag{2}$$

so as to maintain convergence, with the extra degree of freedom of arbitrary phases φ_n.

From (2), it is immediate to examine the way this *Weierstrass–Mandelbrot function* (WFM) behaves under scale changing operations. If, e.g., $\varphi_n = \mu n$, we have $W(\lambda^k t) = \mathrm{e}^{-i\mu k}\lambda^{kH} W(t)$ and, in the special case where $\mu = 0$ (which implies that $\varphi_n = 0$ for all $n \in \mathbb{Z}$), this leads to

$$W\left(\lambda^k t\right) = \lambda^{kH} W(t) \tag{3}$$

for any $k \in \mathbb{Z}$. In this case, the WMF turns out to be *exactly* scale invariant, but *only* with respect to the preferred scaling ratio λ (and any of its integer powers): such a situation is referred to as "discrete scale invariance" (DSI) [20]. If the φ_n's are i.i.d. random variables uniformly distributed on $[0, 2\pi]$, we get a randomized version of the WMF which satisfies a companion form of *statistical* DSI (in the sense of [5])

$$\left\{W\left(\lambda^k t\right),\ t \in \mathbb{R}\right\} \stackrel{d}{=} \left\{\lambda^{kH} W(t),\ t \in \mathbb{R}\right\} \tag{4}$$

for any $k \in \mathbb{Z}$, where the notation "$\stackrel{d}{=}$" stands for equality of all finite-dimensional distributions. A specific interest of such a stochastic version of the WMF (and variations thereof, with Gaussian prefactors) is that it can be used for approximating H-self-similar processes such as fractional Brownian motion [8,15,18].

The specific form of the WMF given in (2) can itself be further generalized to

$$W_g(t) = \sum_{n=-\infty}^{\infty} \lambda^{-nH}\left(g(0) - g\left(\lambda^n t\right)\right)\mathrm{e}^{i\varphi_n}, \tag{5}$$

where $g(t)$ can be any periodic function, provided that it is continuously differentiable at $t = 0$ [21]. Scaling properties of WMF's (2) carry over to their generalized form (5), thereafter referred to as a *generalized WMF* (GWMF).

Typical examples of (G)WMF's are given in Fig. 1.

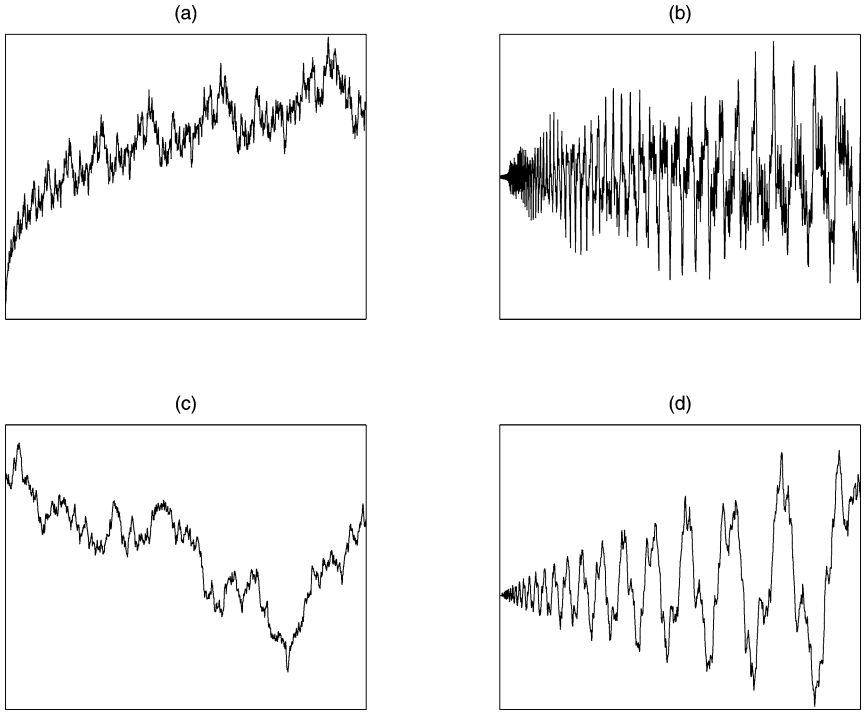

Fig. 1. Examples of Weierstrass–Mandelbrot functions—each graph displays 1000 points of a WMF over the interval $[0, 1]$. Subplots (a) to (c) correspond to the classical WMF defined in Eq. (2), whereas subplot (d) is a generalized WMF as defined in Eq. (5) with $g(t) = \cos^2(t)$. Parameters are as follows: (a) $\lambda = 1.5$, $H = 0.2$, $\varphi_n = 0$; (b) $\lambda = 1.07$, $H = 0.3$, $\varphi_n = n/2$; (c) $\lambda = 1.2$, $H = 0.5$, φ_n i.i.d. over $[0, 2\pi]$; (d) $\lambda = 1.15$, $H = 0.8$, $\varphi_n = n$.

2. Tones vs chirps

2.1. Scale invariance and periodicity

For the above-mentioned suitable choices of phases, the WMF (2) and its generalization (5) are both characterized by two key properties: scale invariance and periodicity. The co-existence of these two properties is made possible because they operate at different levels: periodicity refers to the nature of the building blocks upon which the functions are constructed, whereas scale invariance appears as a result of the superposition. In the stochastic case, the (G)WMF is usually understood as a superposition of processes (e.g., randomly phased tones) which are individually stationary, but whose superposition is not, since it is H-self-similar (as is well known (see, e.g., [19]), stationarity and self-similarity are mutually exclusive properties). In the deterministic case, the periodicity of the individual building blocks is equally broken by the superposition. This remark suggests that there should exist alternative representations for (G)WMF's, based upon scale invariant building blocks rather than periodic or stationary ones. Results of this type can be found in [3,12], but we would like here to adopt a general approach based on a transformation capable of trading stationarity for self-similarity, and vice versa. Such a transformation exists: it is referred to as the *Lamperti transform*.

2.2. The Lamperti transform

Definition 1. Given $H > 0$, the Lamperti transform $\mathcal{L}_H$ operates on functions $\{Y(t),\ t \in \mathbb{R}\}$ according to

$$(\mathcal{L}_H Y)(t) := t^H Y(\log t), \quad t > 0, \tag{6}$$

and the corresponding inverse Lamperti transform $\mathcal{L}_H^{-1}$ operates on functions $\{X(t),\ t > 0\}$ according to

$$\left(\mathcal{L}_H^{-1} X\right)(t) := \mathrm{e}^{-Ht} X\left(\mathrm{e}^t\right), \quad t \in \mathbb{R}. \tag{7}$$

This transform has been first considered by Lamperti in a seminal paper on self-similar processes [14] and it has been later reintroduced independently by a number of authors (see, e.g., [21] or the references quoted in [11]). Whereas various extensions of the Lamperti transform have been recently considered [6,7], the key property of the Lamperti transform—the one which indeed motivated its introduction—is that it allows for a one-to-one correspondence between stationary and self-similar processes or, in an equivalent deterministic context [21], between periodic and self-similar functions.

Periodic functions and stationary processes can naturally be expanded on "tones" (or Fourier modes)

$$\mathrm{e}_f(t) := \mathrm{e}^{i2\pi f t}, \tag{8}$$

whose Lamperti transform expresses straightforwardly as

$$c_{H,f}(t) := (\mathcal{L}_H \mathrm{e}_f)(t) = t^{H+i2\pi f}, \quad t > 0. \tag{9}$$

Such waveforms are referred to as (logarithmic) *chirps* [9], i.e., amplitude and frequency modulated signals of the form $a(t)\exp\{i\psi(t)\}$, with $\psi(t) = 2\pi f \log t$. It thus follows that the derivative of the phase $\psi(t)$ is such that $\psi'(t)/2\pi = f/t$, supporting the idea of a time-varying ("chirping") instantaneous frequency, in contrast with tones whose instantaneous frequency is constant (see Fig. 2). One can remark that logarithmic chirps are a key example of functions exhibiting (discrete) scale invariance (in the sense of (3)) without being fractal: their graph is a smooth function for $t > 0$.

Whereas the tones (8) are the elementary building blocks of the Fourier transform, the chirps (9) are the elementary building blocks of the *Mellin transform* [4] for which we will adopt the following definition:

Definition 2. Given $H > 0$, $\beta \in \mathbb{R}$, and $c_{H,\beta}(t)$ as in (9), the Mellin transform of a function $\{X(t),\ t > 0\}$ is defined by

$$(\mathbf{M}_H X)(\beta) := \int_0^{+\infty} X(t)\overline{c_{H,\beta}(t)}\,\frac{\mathrm{d}t}{t^{2H+1}}, \tag{10}$$

with the corresponding reconstruction formula

$$X(t) = \int_{-\infty}^{+\infty} (\mathbf{M}_H X)(\beta) c_{H,\beta}(t)\,\mathrm{d}\beta. \tag{11}$$

2.3. Chirp decomposition of the GWMF

Based on the different tools that have been introduced, we can now enounce the following proposition, which is the central result of this section:

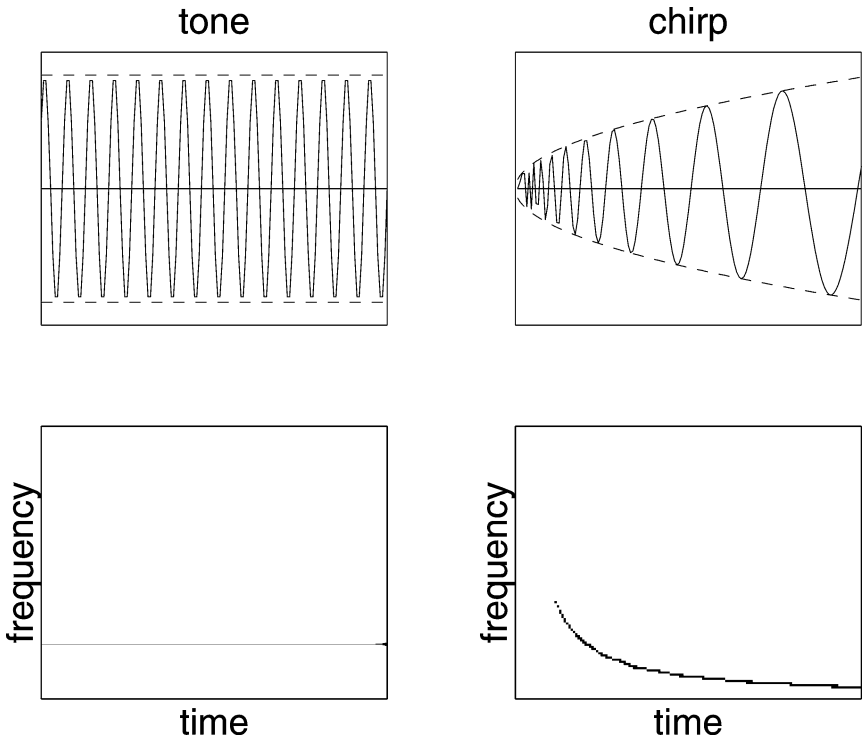

Fig. 2. Tones and chirps—the Lamperti transformation puts in a one-to-one correspondence a tone with a constant amplitude (left column) and a logarithmic chirp with a power-law amplitude (right column). The top row displays examples of such waveforms, and the bottom row the corresponding time–frequency images which evidence and contrast their "instantaneous frequency" structures (constant for the tone and hyperbolic for the chirp).

Proposition 1. *The scale-invariant generalized Weierstrass–Mandelbrot function* (5) *admits the chirp decomposition*

$$W_g(t) = \sum_{m=-\infty}^{\infty} \frac{(\mathbf{M}_H G)(m/\log\lambda)}{\log\lambda} c_{H,m/\log\lambda}(t), \tag{12}$$

with $(\mathbf{M}_H G)(\cdot)$ *the Mellin transform of* $G(t) := g(0) - g(t)$.

Proof. "Delampertizing" the GWMF (5) with $\varphi_n = 0$, we readily get that

$$\big(\mathcal{L}_H^{-1} W_g\big)(t) = \big(\mathcal{L}_H^{-1} W_g\big)(t + k\log\lambda) \tag{13}$$

for any $k \in \mathbb{Z}$, thus proving (as expected) that the inverse Lamperti transform of a scale-invariant GWMF is periodic of period $\log\lambda$. As a periodic function, it can thus be expanded in a Fourier series

$$\big(\mathcal{L}_H^{-1} W_g\big)(t) = \sum_{m=-\infty}^{\infty} w_m \, \mathrm{e}_{m/\log\lambda}(t), \tag{14}$$

with

$$w_m = \frac{1}{\log\lambda} \int_0^{\log\lambda} \left(\mathcal{L}_H^{-1} W_g\right)(t) \overline{\mathrm{e}_{m/\log\lambda}(t)}\, \mathrm{d}t.$$

Inverting (14) and using the fact that the Lamperti transform of a Fourier tone is a chirp (see Eq. (9)), we get

$$W_g(t) = \sum_{m=-\infty}^{\infty} w_m c_{H,m/\log\lambda}(t),$$

with

$$\begin{aligned} w_m &= \frac{1}{\log\lambda} \int_0^{\log\lambda} \left[\mathrm{e}^{-H\theta} \sum_{n=-\infty}^{\infty} \lambda^{-nH} G\left(\lambda^n \mathrm{e}^{\theta}\right)\right] \overline{\mathrm{e}_{m/\log\lambda}(\theta)}\, \mathrm{d}\theta \\ &= \frac{1}{\log\lambda} \sum_{n=-\infty}^{\infty} \lambda^{-nH} \int_{\lambda^n}^{\lambda^{n+1}} G(u)\left(\lambda^{-n}u\right)^{-H} \overline{\mathrm{e}_{m/\log\lambda}(\log u - n\log\lambda)}\, \frac{\mathrm{d}u}{u} \\ &= \frac{1}{\log\lambda} \sum_{n=-\infty}^{\infty} \int_{\lambda^n}^{\lambda^{n+1}} G(u) \overline{c_{-H,m/\log\lambda}(u)}\, \frac{\mathrm{d}u}{u} = \frac{1}{\log\lambda} \int_0^{\infty} G(u) \overline{c_{H,m/\log\lambda}(u)}\, \frac{\mathrm{d}u}{u^{2H+1}} \\ &= \frac{(\mathbf{M}_H G)(m/\log\lambda)}{\log\lambda}, \end{aligned}$$

whence the claimed result. □

One can deduce from this chirp decomposition that the Mellin transform of the GWMF takes on a very simple form, since it reads

$$(\mathbf{M}_H W_g)(\beta) = \sum_{m=-\infty}^{\infty} \frac{(\mathbf{M}_H G)(m/\log\lambda)}{\log\lambda} \delta\left(\beta - \frac{m}{\log\lambda}\right)$$

and thus consists in an infinite series of equispaced peaks. This is the Mellin counterpart of the geometrical comb structure that holds for the Fourier spectrum of the WMF.

Example. As a special case, let us consider the standard WMF (2) with $\varphi_n = 0$. We have in this case $g(t) = \mathrm{e}^{it}$ and

$$w_m = \frac{1}{\log\lambda} \int_0^{\infty} \left(1 - \mathrm{e}^{iu}\right) u^{-s-1}\, \mathrm{d}u,$$

with $s = H + i2\pi m/\log\lambda$. An integration by parts leads to

$$w_m = \frac{\mathrm{e}^{-i\pi/2}}{s} \int_0^{\infty} \mathrm{e}^{iu} u^{(1-s)-1}\, \mathrm{d}u,$$

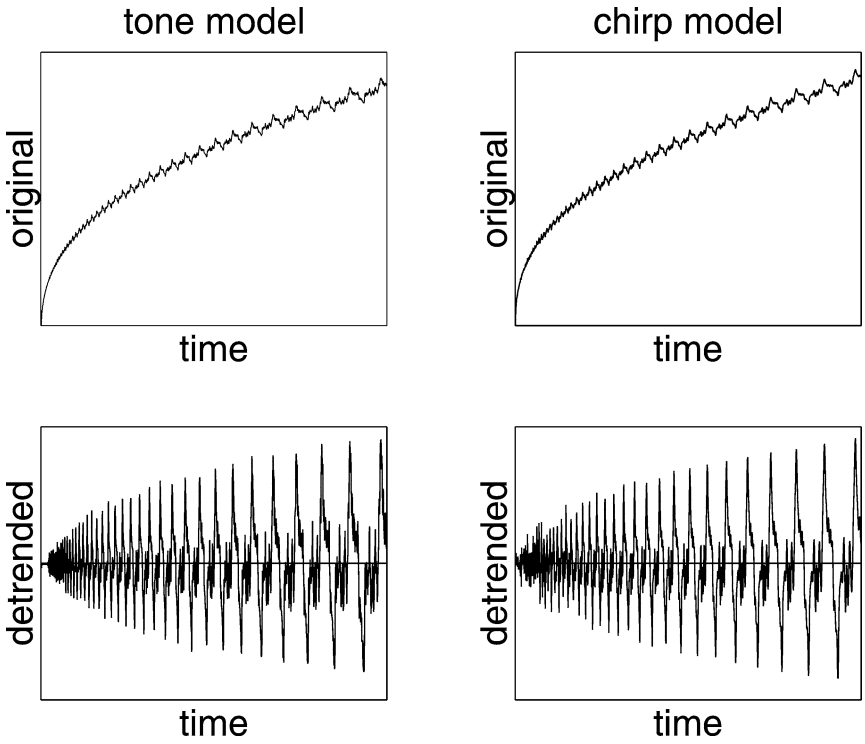

Fig. 3. Tone and chirp models for the WMF—the top row displays 1000 points of a WMF over the interval $[0,1]$, with parameters $\lambda = 1.1$, $H = 0.4$, and $\varphi_n = 0$. The synthesis has been obtained either from the "tone model" (2) with 185 terms (left column) or from the "chirp model" (12) with 20 terms (right column). The bottom row displays the corresponding detrended waveforms.

with $\mathrm{Re}\{1-s\} = 1-H > 0$, thus guaranteeing the convergence of the integral. Making the change of variable $v = u\,\mathrm{e}^{-i\pi/2}$, we finally end up with the result given in [3]

$$w_m = -\frac{1}{\log\lambda}\exp\left\{-i\frac{\pi}{2}\left(H+\frac{i2\pi m}{\log\lambda}\right)\right\}\Gamma\left(-H-\frac{i2\pi m}{\log\lambda}\right), \tag{15}$$

where $\Gamma(\cdot)$ stands for the Gamma function.

Time–frequency interpretation. The so-obtained decomposition can be given a nice interpretation on the time–frequency plane. If we focus, for instance, on the real part of the WMF, the chirp expansion deduced from (12) is comprised of oscillating contributions associated to indexes $m \neq 0$, superimposed to a slowly-varying trend $T_W(t)$ which is captured by the index $m = 0$

$$T_W(t) = \frac{\Gamma(1-H)\cos(\pi H/2)}{H\log\lambda}t^H.$$

An example of the real part of a WMF and its associated detrended graph, obtained from either the standard frequency representation (2) or its chirp counterpart (12), are plotted in Fig. 3, whereas Fig. 4 displays the corresponding time–frequency representations.

Without entering into algorithmic details, one can remark that, depending on which expansion is used, discrete-time synthesis of WMF's is faced with different advantages and drawbacks. In both cases, only a

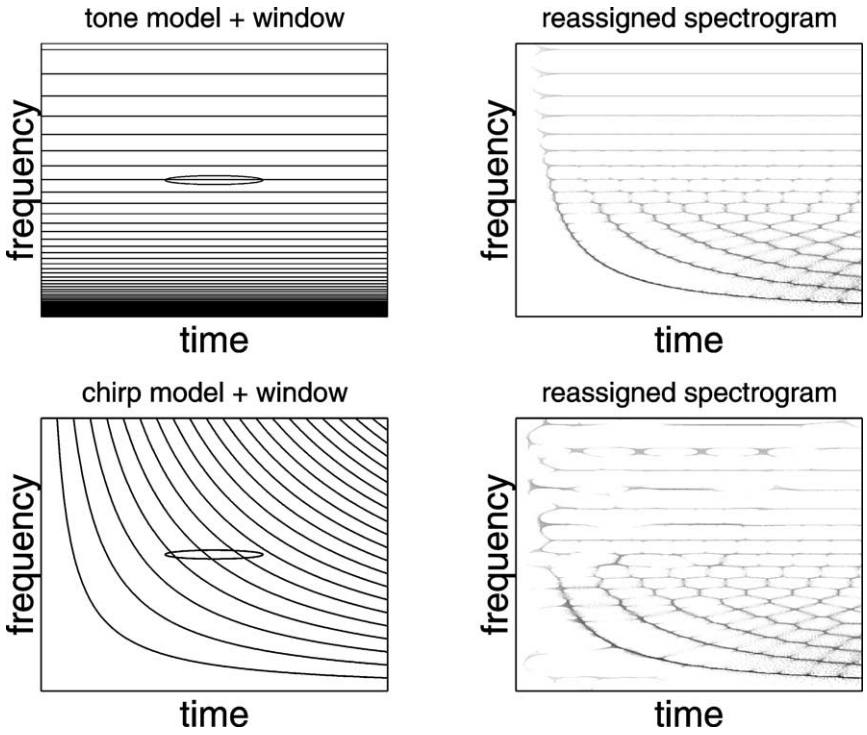

Fig. 4. Time–frequency interpretation of WMF models—idealized time–frequency structures of the WMF models of Fig. 3 are displayed in the left column, together with actual time–frequency distributions in the right column. For a sake of interpretation, one has also superimposed to the left diagrams an ellipse whose dimensions give an indication of the time–frequency window involved in the computation of the (reassigned) spectrograms used for producing the diagrams of the right column. Given a fixed window, it clearly appears that model components (either tones or chirps) are "seen" as such when they enter individually the window. On the contrary, when more than one component is simultaneously "seen" within the window, what the analysis reveals is the result of their superposition: chirps emerge as superimposed tones (top right diagram, lower frequencies), and tones emerge as superimposed chirps (bottom right diagram, higher frequencies).

finite number of terms can be summed up in practice, and frequency limitations occur due to sampling and finite duration effects. If we first think of the lower frequencies, the chirp expansion is clearly favored since the trend is fully taken into account by only one term ($m = 0$), whereas the Fourier expansion would necessitate an infinite number of them (all negative m's). On the contrary, if we think of the higher frequencies, sampling conditions are easily dealt with in the Fourier expansion, whereas all chirps have a priori no built-in frequency limitation. This explains why the two waveforms of Fig. 3 are not fully identical.

For a sake of improved localization on chirps, we used as time–frequency representations reassigned spectrograms [1,2] which basically perform a Fourier analysis on a short-time basis. As is well known, a spectrogram and its reassigned version are naturally equipped with a "time–frequency window" whose dimensions are determined by the equivalent duration and spectral width of some a priori chosen short-time window. Therefore, if we superimpose the occupation area of this time–frequency window to the idealized WMF models of Eq. (2) (which consists of geometrically spaced spectral lines) and Eq. (12) (which consists of chirps), we clearly see that different regimes may be observed, depending on the way

spectral lines and chirps are "seen" through the window. Given a fixed spectral width for the window, spectral lines will be considered as natural individual components as long as their spacing will be large enough to not allow more than one line to enter the window at the same time: this is what we observe for sufficiently high frequencies. On the contrary, when many spectral lines are simultaneously present in the window, what time–frequency analysis reveals in the result of the superposition, i.e., chirps: this is what we observe at lower frequencies. Reasoning along the same lines leads to the same result if we replace the "tone model" (2) by the "chirp model" (12). In this case, the perspective is reversed and spectral lines appear at high frequencies as the result of the co-existence of multiple chirps within the time–frequency window, whereas the emergence of chirps is privileged at lower frequencies, where they are dealt with individually.

2.4. The case of randomized WMF's

The underlying chirp structure that has been evidenced for deterministic GWMF's can be viewed as a result of the fixed phase relationships which exist between the constitutive tones. In particular, in the simplest case where $\varphi_n = 0$ for all n's, all tones are in phase at time $t = 0$, with the consequence that the time origin plays a very specific role. In the case where the phases φ_n are i.i.d. random variables, the picture is drastically changed, and no coherent phase organization can be expected to occur in individual realizations of randomized GWMF's. However, this limitation does not prevent from still identifying chirps in quantities related to ensemble averages, and the task proves to be made easy by the fact that, while being nonstationary processes, randomized GWMF's (in particular, WMF's) may turn out to have stationary increments.

More precisely, given $\theta > 0$, we will introduce a θ-increment operator by its action on a function $X(t)$ according to

$$(\Delta_\theta X)(t) := X(t+\theta) - X(t).$$

Assuming that the phases φ_n are i.i.d. random variables uniformly distributed on $[0, 2\pi]$, it follows immediately from (5) that the corresponding θ-increment process is zero-mean, i.e., that $\mathbb{E}(\Delta_\theta W_g)(t) = 0$. Second-order properties of $(\Delta_\theta W_g)(t)$ can be evaluated as well, leading to

$$\mathbb{E}(\Delta_\theta W_g)(t)\overline{(\Delta_\theta W_g)(s)} = \sum_{n=-\infty}^{\infty} \lambda^{-2nH} (\Delta_{\lambda^n\theta} G)\big(\lambda^n t\big)\overline{(\Delta_{\lambda^n\theta} G)\big(\lambda^n s\big)}, \tag{16}$$

with $G(t) = g(0) - g(t)$ as previously. In particular, the variance can be simply expressed as

$$\mathbb{E}\big|(\Delta_\theta W_g)(t)\big|^2 = \sum_{n=-\infty}^{\infty} \lambda^{-2nH} \big|(\Delta_{\lambda^n\theta} G)\big(\lambda^n t\big)\big|^2. \tag{17}$$

Further simplications can be obtained in the specific case of the WMF $W(t)$ for which $g(t) = \mathrm{e}^{it}$, since we then have $|(\Delta_{\lambda^n\theta} G)(\lambda^n t)|^2 = |1 - \mathrm{e}^{i\lambda^n\theta}|^2$ for all t's, from which it follows that:

$$\mathbb{E}\big|(\Delta_\theta W)(t)\big|^2 = 2\sum_{n=-\infty}^{\infty} \lambda^{-2nH}\big(1 - \cos\lambda^n\theta\big). \tag{18}$$

As a function of time t, the variance of the θ-increments of randomized WMF's is therefore a quantity which is constant. As a function of the increment step θ, the same quantity (which can also be referred

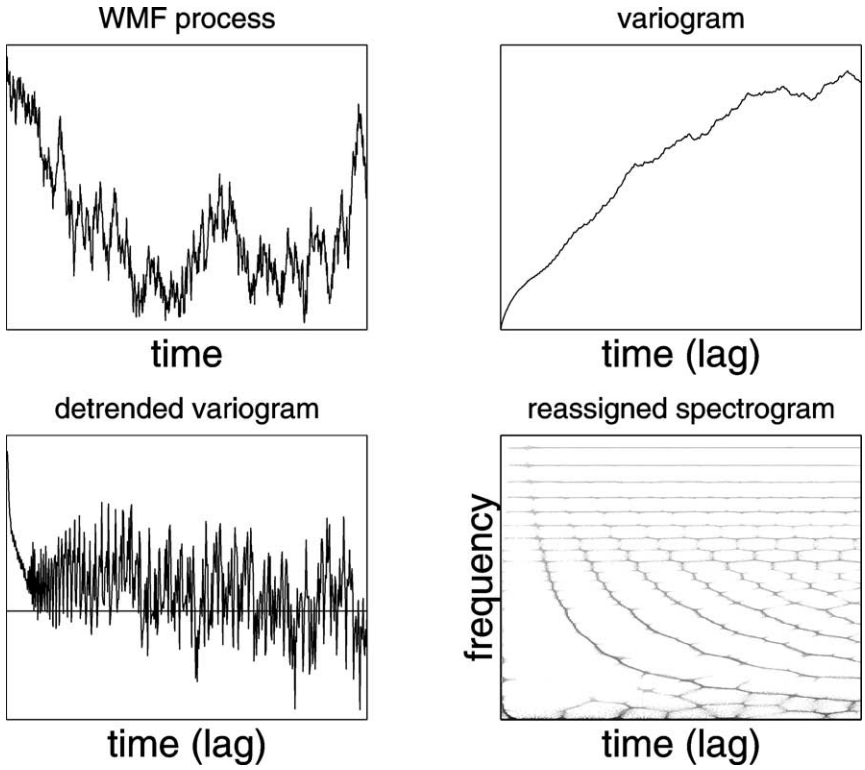

Fig. 5. Variogram of randomized WMF—in the case of a randomized WMF, the ensemble averaged variogram is expected to be itself a WMF. When dealing with one realization (top left diagram, in this case $\lambda = 1.07$, $H = 0.3$, and φ i.i.d. over $[0, 2\pi]$), one can estimate an empirical variogram from the 1000 observed data points (top right). Detrending this estimate by a first-order differencing operator (bottom left) gives a function whose time–frequency analysis (bottom right) reveals the mixed structure of tones and chirps observed in deterministic WMF's (see Fig. 4).

to as a *variogram*, or a *second-order structure function*) is nothing but (twice) the real part of the deterministic WMF (2), with exponent $2H$ and phases $\varphi_n = 0$. Since the variogram is itself a WMF, it can be expanded on chirps and the results given previously for deterministic WMF's apply. Figure 5 gives an example of a randomized WMF, together with an empirical estimate of its variogram. The simulation consisting of a discrete-time approximation $\{W_g[n],\ n = 1, \ldots, N\}$, the variogram estimate is simply given by

$$\hat{V}[k] = \frac{1}{N-k} \sum_{n=1}^{N-k} \left| W[n+k] - W[n] \right|^2, \quad k = 0, \ldots, K, \tag{19}$$

with $K \ll N$ so as to guarantee a statistical significance to the estimation. In theory, i.e., if the variogram was indeed evaluated via an ensemble average in place of the time average (19), a trend removal could be applied in closed form, as in the deterministic case. When dealing with only one realization, this is unfortunately no more possible but, based upon the reasonable assumption that the trend, yet different from one realization to the other, has a significantly slower evolution than the oscillating chirp components, a poorman's substitute can be proposed by simply computing $(\Delta_1 V)[k]$. The outcome of

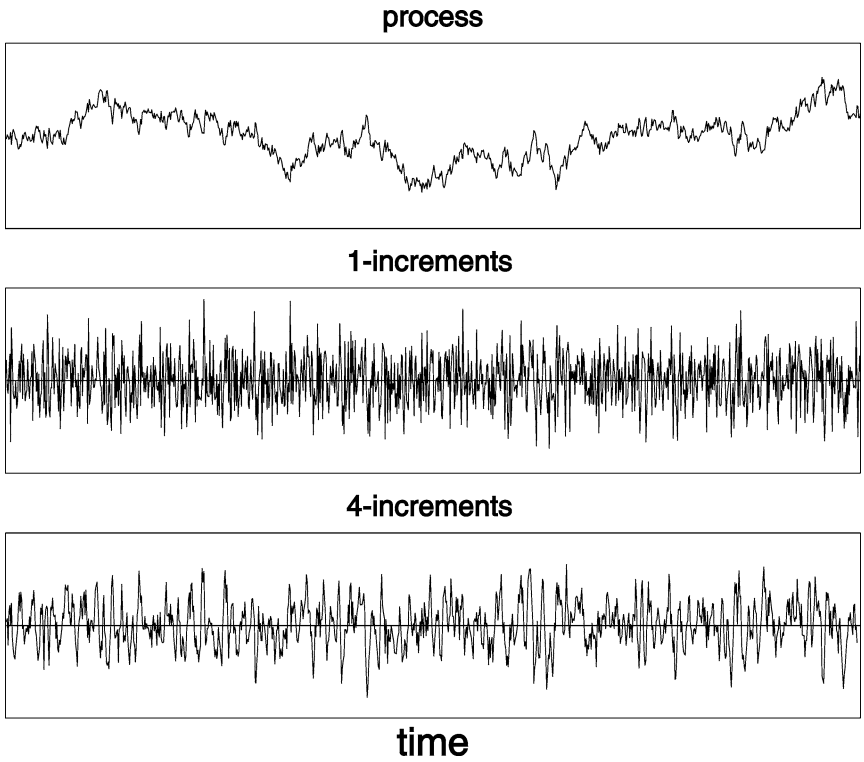

Fig. 6. WMF and increments—the top graph displays 1000 points of a WMF over the interval $[0, 1]$, with parameters $\lambda = 1.07$, $H = 0.3$, and φ_n i.i.d. over $[0, 2\pi]$. The two graphs below display the corresponding increment processes obtained with increment steps 1 and 4, respectively. Both are stationary processes.

this crude simplification is plotted in Fig. 5, together with the corresponding time–frequency analysis, which can be compared with profit to those of Fig. 4.

Still restricting to the WMF case, the companion specification of the two-point correlation function (16) gives

$$\mathbb{E}(\Delta_\theta W)(t)\overline{(\Delta_\theta W)(s)} = 2\sum_{n=-\infty}^{\infty} \lambda^{-2nH}\left(1-\cos\lambda^n\theta\right)\mathrm{e}^{i\lambda^n(t-s)}, \tag{20}$$

a function which only depends on the difference $t - s$, thus guaranteeing that the θ-increments process $(\Delta_\theta W)(t)$ is second-order stationary for any θ.

Denoting by $R_\theta(\tau)$ the real part of the corresponding stationary autocorrelation function $\mathbb{E}(\Delta_\theta W)(t) \times \overline{(\Delta_\theta W)(t+\tau)}$, we do not get (for a fixed θ) a quantity which would be exactly scale-invariant as a function of τ. However, comparing the real part of (20) with (1), we observe that it corresponds to a WF of a similar type, properly extended to negative n's by weighting each Fourier mode $\cos\lambda^n\tau$ of amplitude λ^{-2nH} by a regularizing term $(1-\cos\lambda^n\theta)$: we get therefore an approximate form of scale invariance which depends on the increment step θ. For a fixed λ, a larger θ tends to increase the relative contribution of negative n's in the sum, i.e., to enhance lower frequencies. An illustration of this fact is given in Figs. 6 and 7 where, proceeding as for the variance and noting that the autocorrelation function

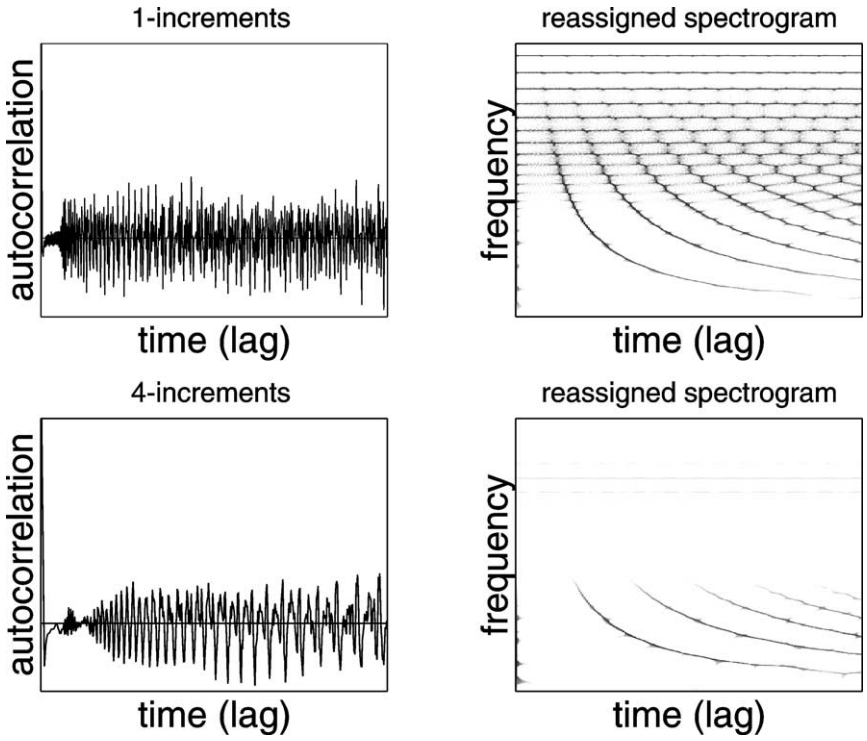

Fig. 7. Autocorrelation of WMF increment processes—the left column displays the empirical autocorrelation estimates for the (stationary) WMF increment processes considered in Fig. 6. The right column displays the corresponding time–frequency images, supporting the expectation that such quantities undergo an approximate self-similar behavior, close to that of a WMF, with a relative contribution of lower frequencies which is reinforced when the increment step is made larger.

of $\mathrm{Re}\{(\Delta_\theta W)(t)\}$ and $\mathrm{Im}\{(\Delta_\theta W)(t)\}$ are identical and both equal to $R_\theta(\tau)/2$, we used the empirical estimate

$$\widehat{R_m}[k] = \frac{2}{N-k}\sum_{n=1}^{N-k} \mathrm{Re}\big\{W[n+m]-W[n]\big\}\,\mathrm{Re}\big\{W[n+m+k]-W[n+k]\big\}.$$

3. Concluding remarks

The results presented here were intended to shed a new light on alternative chirp decompositions that may be used for representing (generalized) Weierstrass–Mandelbrot functions. Special emphasis has been put on a time–frequency interpretation according to which both tones and chirps equally exist as constitutive building blocks of GWMF's, and can be revealed by an adapted analysis. As such, time–frequency analysis appears as a powerful tool which can be applied to other types of functions in order to evidence in a simplified way the existence of a rich inner structure in a waveform (one can, e.g., report to [10] for an application of the same technique to Riemann's function). One can also think of further extensions related directly to the basic formulation (2) (e.g., the "non-chiral" extensions pushed forward in [17]), or to the chirp expansion (12) (for which it is worth stressing the fact that a number

of results have already been obtained about different behaviors and their classification, depending on the structure of amplitude and phase terms [12]). In the classical formulation (5), GWMF's appear as an extension of (2) in which tones are replaced by other *functions* whereas, in the chirp formulation (12), the same extension relies in a simpler way on a modification of *coefficients*, leaving room to additional manipulations on the chirps themselves (e.g., by making use of a collection of different H's). This may pave the road to newly controlled variations on the WMF and its (old and new) generalizations.

References

[1] F. Auger, P. Flandrin, Improving the readability of time–frequency and time-scale representations by the reassignment method, IEEE Trans. Signal Proc. SP-43(5) (1995) 1068–1089.
[2] F. Auger, P. Flandrin, P. Gonçalvès, O. Lemoine, Time–frequency toolbox for MATLAB, user's guide and reference guide. Freeware available at: http://iut-saint-nazaire.univ-nantes.fr/~auger/tftb.html.
[3] M.V. Berry, Z.V. Lewis, On the Weierstrass–Mandelbrot fractal function, Proc. Roy. Soc. London A 370 (1980) 459–484.
[4] J. Bertrand, P. Bertrand, J.Ph. Ovarlez, The Mellin transform, in: A. Poularikas (Ed.), The Transforms and Applications Handbook, CRC Press, 1990.
[5] P. Borgnat, P. Flandrin, P.-O. Amblard, Stochastic discrete scale invariance, IEEE Signal Process. Lett. 9 (6) (2002) 181–184.
[6] P. Borgnat, Modèles et outils pour l'invariance d'échelle brisée: Variations sur la transformation de Lamperti et contributions aux modèles statistiques de vortex en turbulence, PhD thesis (in French), École Normale Supérieure de Lyon, France, 2002.
[7] P. Borgnat, P.-O. Amblard, P. Flandrin, Lamperti transformation for finite size scale invariance, in: Proc. Internat. Conf. on Physics in Signal and Image Proc. PSIP-03, Grenoble, 2003, pp. 177–180.
[8] K. Falconer, Fractal Geometry, Wiley, 1990.
[9] P. Flandrin, Time–Frequency/Time-Scale Analysis, Academic Press, 1999.
[10] P. Flandrin, Time–frequency and chirps, Wavelet Applications VIII, SPIE, Vol. 4391, in: Proc. of AeroSense'01, Orlando, FL, 2001.
[11] P. Flandrin, P. Borgnat, P.-O. Amblard, From stationarity to self-similarity, and back: Variations on the Lamperti transformation, in: G. Raganjaran, M. Ding (Eds.), Processes with Long-Range Correlations, Springer, 2003, in press.
[12] S. Gluzman, D. Sornette, Log-periodic route to fractal functions, Phys. Rev. E 6503 (3) (2002) T2A:U418–U436.
[13] G.H. Hardy, Weierstrass's non-differentiable function, Trans. Amer. Math. Soc. 17 (1916) 301–325.
[14] J. Lamperti, Semi-stable stochastic processes, Trans. Amer. Math. Soc. 104 (1962) 62–78.
[15] B.B. Mandelbrot, J.W. Van Ness, Fractional Brownian motions, fractional noises and applications, SIAM Rev. 10 (1968) 422–437.
[16] B.B. Mandelbrot, Fractals: Forms, Chance and Dimension, Freeman, 1977.
[17] B.B. Mandelbrot, Gaussian Self-Affinity and Fractals, Springer, 2002.
[18] V. Pipiras, M.S. Taqqu, Convergence of the Weierstrass–Mandelbrot process to fractional Brownian motion, Fractals 8 (2000) 369–384.
[19] G. Samorodnitsky, M.S. Taqqu, Stable Non-Gaussian Random Processes: Stochastic Models with Infinite Variance, Chapman and Hall, 1994.
[20] D. Sornette, Discrete scale invariance and complex dimensions, Phys. Rep. 297 (1998) 239–270.
[21] C. Tricot, Courbes et Dimension Fractale, Springer, 1993.
[22] K. Weierstrass, Über continuirliche Functionen eines reelles Arguments, die für keinen Werth des letzteren einen Bestimmten Differentialquotienten besitzen, Königl. Akademie der Wissenschaften, Berlin, July 18, 1872;
Reprinted in: K. Weierstrass, Mathematische Werke II, Johnson, New York, 1967, pp. 71–74.